A first-principles study of electron–phonon coupling in electron-doped LiH

2007 J. Phys.: Condens. Matter 19 425218

(http://iopscience.iop.org/0953-8984/19/42/425218)

IOP PUBLISHING JOURNAL OF PHYSICS: CONDENSED MATTER

J. Phys.: Condens. Matter **19** (2007) 425218 (10pp) doi:10.1088/0953-8984/19/42/425218

A first-principles study of electron–phonon coupling in electron-doped LiH

J Y Zhang, L J Zhang, T Cui, Y L Niu, Y M Ma[1], Z He and G T Zou

National Laboratory of Superhard Materials, Jilin University, Changchun 130012, People's Republic of China

E-mail: mym@jlu.edu.cn

Received 3 August 2007
Published 18 September 2007
Online at stacks.iop.org/JPhysCM/19/425218

Abstract

The electronic structure, lattice dynamics, and electron–phonon coupling (EPC) of electron (n)-doped LiH have been extensively studied using *ab initio* methods within the virtual crystal approximation. The overall agreement of the lattice constants and bulk modulus for pure LiH with the experiments is excellent if the zero-point motion is taken into account. From the theoretical calculation for n-doped LiH, it is indicated that metallic n-doped LiH might be a good superconductor. Moreover, the EPC parameter λ for n-doped LiH was found to increase with the dopant concentration, resulting from the softening of optical phonon modes and the increase of the electron density of states at the Fermi level, while a decreasing trend of λ was predicted for the presence of pressure. Phonon linewidth calculations suggested that the optical phonon mode makes the main contribution to the EPC. A possible mechanism for the predicted superconductivity of n-doped LiH has been discussed.

(Some figures in this article are in colour only in the electronic version)

1. Introduction

Lithium hydride has been extensively studied as the most elementary ionic compound since the early days of solid-state theory because of the important usage in thermonuclear material and potential energy supply. Lithium hydride is the simplest alkali hydride, possibly the simplest compound material, and its electronic and structural properties have been the subject of extensive investigation [1–4]. Despite its electronic simplicity, subtle physics has been revealed with the effects of partial covalent bonding and large zero-point motion [5].

The search for possible superconducting materials is a subject of topical interest. Low Z materials are beneficial for increasing the superconducting transition temperature because of

[1] Author to whom any correspondence should be addressed.

their high Debye temperatures. It is known that the Li atom and the H atom have strikingly light atomic masses. Correspondingly, LiH would have a very high Debye temperature Θ_D, which might potentially yield superconductivity, as deduced from the famous McMillan formula [6]: $T_c = \frac{\Theta_D}{1.45}[\frac{-1.04(1+\lambda)}{\lambda(1-0.62\mu^*)-\mu^*}]$. It is well known that a superconductor should be a conductor first. However, for the case of LiH, it is a semiconductor with a large band gap of ∼5 eV [7, 8] at ambient pressure. Generally, there are two efficient ways to make LiH a metal. One is to impose high pressure on the material to close its band gap. The other one is through a doping process. For the former case, even if we increase the pressure up to 500 GPa in the rocksalt phase in our simulation, a band gap of 0.2 eV still exists. In practice, pressure beyond 500 GPa is almost the experimental limit at the current stage. Also, even it becomes a metal under strong compression, how one keeps the metallic states after the pressure is released is still a challenging issue. Therefore, as a preferable alternative, the doping process becomes more feasible for making LiH a metallic state. Due to the extremely small atomic mass, substitution of H is not a trivial issue, while a substitution of Li with Be, Mg, and Ca might, therefore, be more realistic. For these types of doping, the dopant acts as a donor which donates electrons to the system.

The current study is the first theoretical effort at exploring the possible superconductivity in n-type LiH. A virtual crystal approximation (VCA) [9] was used to model the electronic state, vibrational properties, and the EPC for n-type LiH with different concentrations of dopants. In our previous work [10], a possible mechanism for superconductivity in hole- and electron-doped diamonds has been successfully discussed within the VCA.

2. Computational details

Pseudopotential plane-wave *ab initio* calculations were performed within the framework of density functional theory [11, 12]. The core–valence electron interaction is described by both norm-conserving and ultrasoft pseudopotentials with a Perdew–Burke–Ernzerhof (PBE) [13] exchange–correlation (XC) functional. It should be pointed out that due to the relatively large size of the alkali core, the decoupling of the electronic charge into a core and a valence contribution is more problematic than for most of the other atoms in the periodic table, and non-linear core correction (NLCC) to the XC energy functional should be adopted in order to obtain sensible results. We introduced the NLCC to the XC energy functional to generate pseudopotentials for Li. The electronic wavefunctions and charge densities were expanded in plane-wave basis sets. To test convergence with respect to these choices, we repeated several other calculations using pseudopotentials with different k-mesh and kinetic energy cut-off. Convergence tests gave the kinetic energy cut-off, $E_{\mathrm{cut-off}}$, as 60 Ryd and an $8 \times 8 \times 8$ Monkhorst–Pack (MP) [14] grid (k-mesh) for the electronic Brillouin zone integration. The lattice dynamics for these compounds was investigated by using the linear response method, which has been successfully applied to the computation of phonon dispersion in insulators [12] and metals [15, 16], and to the computation of EPC [17]. BZ integrations are performed using Methfessel–Paxton smearing [18] with a linewidth of 0.05 Ryd. A $12 \times 12 \times 12$ MP k-mesh was found to yield phonon frequencies converged to within 0.05 THz. A $4 \times 4 \times 4$ k mesh in the first BZ was used in the interpolation of the force constants for the phonon dispersion curve calculations. Dynamical matrices on this grid have been calculated and the real-space interatomic force constants were obtained by inverse Fourier transformation. The complete phonon dispersion curves were then obtained by interpolating the dynamical matrices using these force constants. A MP $24 \times 24 \times 24$ k-mesh was used to ensure k-point sampling convergence with Gaussians of width 0.04 Ryd, which approximates the zero-width limits in the calculations of phonon linewidth and EPC parameter λ. The linewidth of the phonon mode

Table 1. Calculated equilibrium lattice parameter (a_0) and bulk modulus (B_0) for pure LiH with different pseudopotentials. The experimental data [2] in parentheses are also listed for comparison. The units for a_0 and B_0 are au and GPa, respectively. NC and US are the abbreviations for norm-conserving and ultrasoft pseudopotentials.

	GGA			LDA	
	PBE (NC)	PW (NC)	PW (US)	PZ (NC)	PZ (US)
a_0 (au)	7.43(7.67)	7.44	7.60	7.38	7.43
B_0 (GPa)	34.03(34.24)	38.20	39.99	41.33	42.80

j at wavevector q, $\gamma_{q,j}$, arising from electron–phonon interaction is given by [19–21]

$$\gamma_{qj} = \frac{4\pi\omega_{qj}}{N_k} \sum_{knm} \left| g^j_{kn,k+qm} \right|^2 \delta(\varepsilon_{kn})\delta(\varepsilon_{k+qm}) \tag{1}$$

where the sum is over the BZ, N_k is the number of k-points in the sum, and ε_{kn} are the energies of bands measured with respect to the Fermi level at point k. $g^j_{kn,k+qm}$ is the electron–phonon matrix element. The EPC constant λ is defined as $\lambda_{qj} = \frac{\gamma_{qj}}{\pi\hbar N_f \omega^2_{qj}}$ where N_f is the electron density of states (DOS) per atom and spin at the Fermi level ε_f. The electron–phonon mass enhancement parameter λ can be defined as the first reciprocal moment of the spectral function $\alpha^2 F(\omega)$ [19–21]:

$$\lambda = 2\int_0^\infty \frac{\alpha^2 F(\omega)}{\omega}\,\mathrm{d}\omega \approx \sum_{qj} \lambda_{qj} w(q) \tag{2}$$

where $w(q)$ is the weight of a q-point in the first BZ. We substituted a Gaussian for the δ function in equation (1).

3. Results and discussion

The theoretical equilibrium lattice constant is determined by fitting the total energy as a function of volume to the Murnaghan equation of states (EOS) [22]. The calculated equilibrium lattice parameters and bulk modulus, together with the calculations using other pseudopotentials whose XC functionals are Perdew–Wang 91 (PW91) [23], the generalized gradient approximation (GGA), Perdew–Zunger (PZ) [24] and local density approximation (LDA) respectively, and the experimental data [2] are listed in table 1. It is clear that the current theoretical lattice constants and bulk modulus are in good agreement with experimental data. The reasonable agreement between experiment and theory strongly supports the choice of pseudopotentials. It should be pointed out that the results obtained with the pseudopotential within the PBE XC functionals are the best among the different choices of pseudopotential in view of the excellent agreement with the experiment in the bulk modulus. Thus, this pseudopotential was mainly used in the current study. The calculated EOS of pure LiH in rocksalt structure is compared with the experimental data [4] as shown in figure 1. The agreement between theoretical results and the experimental data is also excellent, lending further strong support to the validity of the current theoretical model. Assuming the replacement of a Li atom with a donor atom (e.g., beryllium doping) contributes exactly one electron in the conduction band, the estimated dopant concentration (dc) is summarized in table 2. The calculated lattice constant with the inclusion of zero-point motion and bulk moduli with dc for pure and n-doped LiH are also listed in table 2. The introduction of electrons reduces

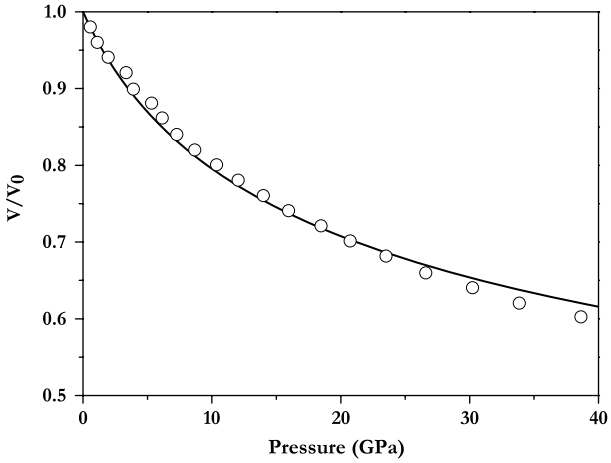

Figure 1. Comparison of the calculated equation of state (solid line) for LiH (solid circle symbols) with the experimental data [4].

Table 2. Calculated lattice constant (a_0), bulk modulus (B_0), average phonon frequency ($\langle\omega\rangle$), density of states at the Fermi level ($N(0)$), EPC coefficient (λ), logarithmically averaged characteristic phonon frequency ($\omega_{\log}$), and superconducting transition temperature (T_c) for n-doped LiH with $e_v = 2.02$, 2.03, 2.04, 2.05, and 2.06.

LiH	e_v	dc (%)	a_0 (au)	B_0 (GPa)	$\langle\omega\rangle$ (THz)	$N(0)$ (states Ryd^{-1} /spin· unit cell)	λ	$\omega_{\log}$ (K)	T_c (K)
Pure	2.00		7.63	34.03	16.94				
n-type	2.02	2.00	7.65	32.56	16.63	0.52	0.22	518.18	0.00
	2.03	3.00	7.67	31.60	16.45	0.64	0.27	497.27	0.09
	2.04	4.00	7.71	31.30	16.05	0.74	0.36	423.30	0.96
	2.05	5.00	7.74	30.73	15.75	0.81	0.44	355.83	2.85
	2.06	6.00	7.81	30.58	15.32	0.87	0.86	143.24	7.78

the chemical bonding as evidenced by the increase of the lattice constant and the decrease of bulk modulus with dc as shown in table 2.

Anharmonic effects make phonon frequencies depend upon the crystal volume. As a consequence, the zero-point energy contribution to the crystal energy affects the values of the equilibrium lattice spacing and bulk modulus. In order to evaluate the zero-point energy as a function of volume, we have performed the same method as was proposed by Roma *et al* [25] within density functional perturbation theory (DFPT) calculations of phonon frequencies with nine different volumes at eight generic q-points in the irreducible wedge of the BZ corresponding to a uniform $4 \times 4 \times 4$ q-mesh, from which we could calculate the energy contribution from the zero-point motion as

$$E_{ZP} = \tfrac{1}{2} \sum_{j,q} \hbar\omega_j^q(V) \tag{3}$$

and fit $E_{ZP}(V)$ to obtain the zero-point energy at different volumes. The inclusion of zero-point motions in the total energy results in an improved agreement between the calculations and experiments. The equilibrium lattice constant is increased from 7.43 to 7.63 au, which is

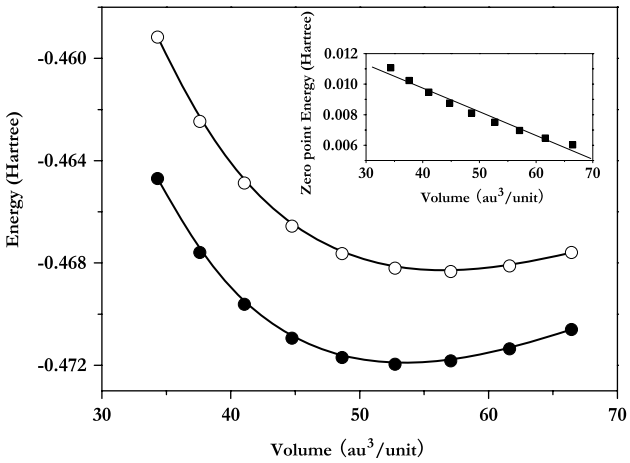

Figure 2. Total energies of LiH as a function of the unit cell volumes. Main figure: open and solid circles are the results with and without the inclusion of zero-point motions. Inset: the zero-point energy with volume. Lines are the fitted curves.

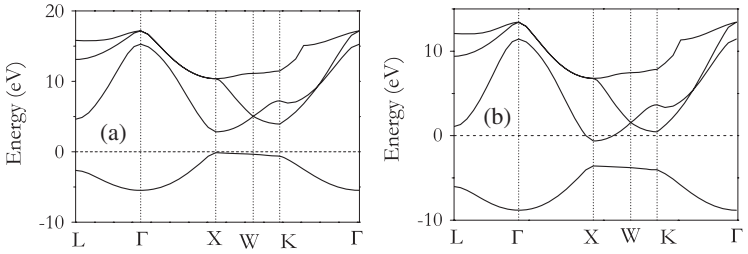

Figure 3. The calculated band structures for pure (a) and n-doped (b) LiH with $e_v = 2.04$. The horizontal dashed line denotes the Fermi level.

closer to the experimental value 7.67, as listed in table 2 and shown in figure 2; thus the phonon frequencies were calculated at the corresponding cell volumes with the lattice constants listed in table 2.

The electronic band structure for pure and n-doped LiH with $e_v = 2.04$ is shown in figure 3. The band structure presents a direct energy band gap of 3.05 eV at the X point, much lower than the experimental value ≈5 eV [7, 8] characteristic of GGA calculations, but a bit larger than 2.14 eV reported by Kunc *et al* [26], probably as a consequence of the inclusion of zero-point motion which results in a larger lattice constant. The band structure of n-doped LiH with $e_v = 2.04$ also reveals that the electrons introduced into the conduction band help to increase the electron density near the X point at the Fermi level and make n-doped LiH weakly metallic. The electron DOS for n-doped LiH at the Fermi level, $N(0)$, increases with dc as shown in table 2.

It is known that the VCA excludes the possibility of wavefunction localization on particular atoms by insisting that all anions in an alloy are identical (to a 'virtual' anion), and by neglecting atomic relaxation. To avoid this discrepancy and test the applicability of the VCA to the n-type LiH system, we also use the supercell technique [27, 28] which is good at mimicking local chemical properties for modelling n-doped LiH. In order to study the metallic state of n-doped LiH with dc we choose two models: $2 \times 2 \times 2$ LiH supercells within the conventional and

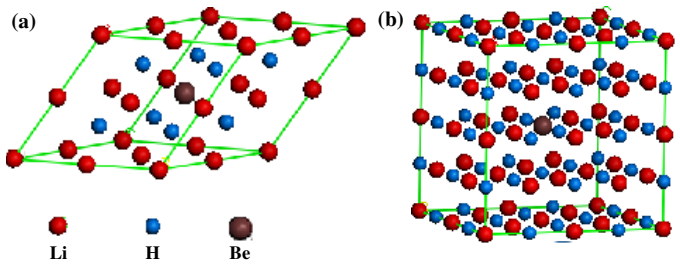

Figure 4. Structures of (a) model I and (b) model II. Please refer to the text for the description of the models.

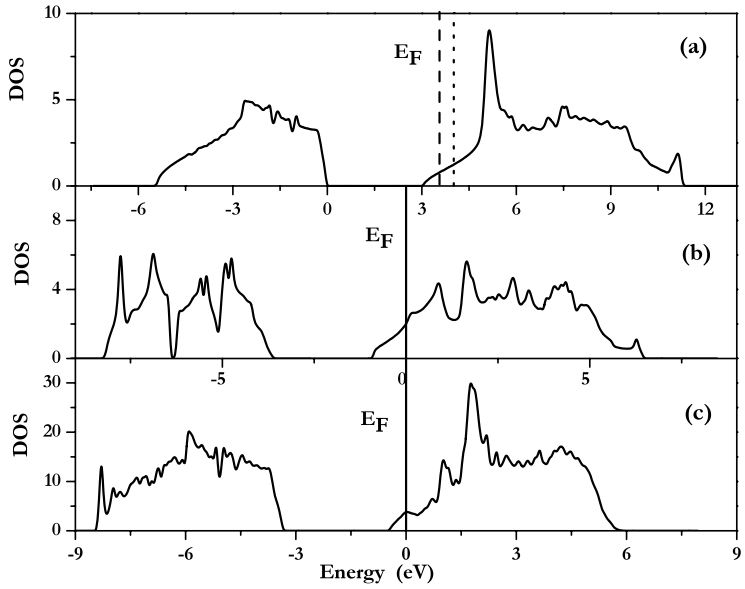

Figure 5. Electronic DOS for the undoped and the two beryllium-doped LiH supercells. (a) The TDOS of the undoped LiH. (b), (c) The TDOS plots for models I and II. The TDOS is in states $\mathrm{eV}^{-1}/\mathrm{spin}\cdot\mathrm{unit\ cell}$. The dashed and dotted vertical lines in (a) show the Fermi level E_F simulated by the VCA methods with dc values of 2% and 6%, respectively (for the pure LiH, the valence band top is taken as the Fermi level).

primitive cells, respectively, with a Li atom substituted by a Be atom, named models I and II, shown in figure 4. The dc values for models I and II are 6.25% and 1.56%, respectively, which cover the dc range considered in the VCA study. We fully relax the unit cell by minimizing the atomic strain energy. This type of calculation allows for the following physical effects: (1) wavefunction localization, (2) atomic relaxation, (3) multiband coupling, (4) the existence of a distribution of many local chemical environments. Then, we compute the total electronic density of states (TDOS) for the two optimized supercells.

The TDOS for models I and II are plotted in figure 5. The TDOS apparently indicates a metallic behavior for both doped models, contrasting with the semiconducting behavior of the pure LiH. The TDOS for model I is very similar to that for model II, except showing more metallic behavior as evidenced by a larger $N(0)$. The metallization in the n-doped LiH is from

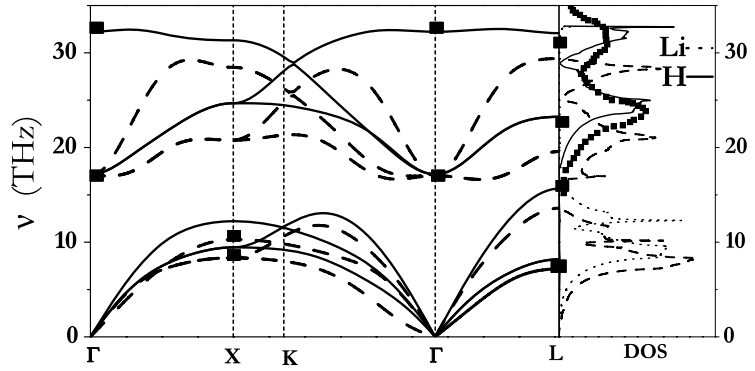

Figure 6. Calculated phonon dispersion curves (left panel) and hydrogen projected PDOS (right panel) for pure and doped ($e_v = 2.06$) LiH together with the experimental data. Solid squares in the left and right panels are the experimental data taken from [25] and [29], respectively. Solid and dashed lines in the left panel are the calculated results for pure and doped LiH respectively. Solid and dotted lines in the right panel are the theoretical hydrogen and lithium projected phonon density of states for pure LiH, respectively, while the dashed line represents the PDOS for doped LiH.

the doping of beryllium as expected. It is very important that both delocalized (VCA) and localized (supercell model) defects did give qualitatively similar descriptions of the metallic behaviors for mimicking the doped LiH. The Fermi energy levels simulated with supercell models are 0.5 eV and 0.92 eV higher than the conduction band minimum (CBM) with dc values of 1.56% and 6.25% respectively, while results from the VCA are 0.45 and 0.84 eV higher than the CBM ones. The Fermi energy positions given by the two supercell models are consistent with our VCA calculation results with dc values of 2% and 6% respectively, the negligible discrepancy being due to the dc differences, which are shown in figure 5(a).

The left panel of figure 6 shows the comparison of the calculated phonon dispersion curves with the experimental data (solid squares) [25] for pure and doped ($e_v = 2.06$) LiH. The very high phonon frequencies in the doped LiH (up to 30 THz) may lead to a strong electron–phonon interaction. With the addition of the non-analytic term to the dynamical matrix, the longitudinal optic (LO) phonon branch and the transverse optic (TO) phonon branch split from each other at the Γ point in the pure LiH, and this is shown. It is clear that the calculated phonons at several high symmetry points, Γ, X, and L, in the BZ are in good agreement with experimental data [25] (deviations $\leqslant$6%). It should be pointed out that the LO and TO branches do not split from each other at the zone center, signifying a metallic state. With the introduction of the dopant, the phonon dispersion was predicted to be significantly softened along all the directions as shown in the figure 6. This behavior might be closely related to the increase in lattice constant with doping as listed in table 2. It is noteworthy that the phonon softening behavior will contribute to the increased EPC. The right panel in figure 6 shows the calculated projected phonon density of states (PDOS) together with the experimental data [29]. It is important to note that the H atom makes the main contribution to the high frequency vibrations because of its relatively light atomic mass, as expected. One observes that the theoretical hydrogen projected phonon DOS agrees well with the experimental data. Specifically, two main peak positions are well reproduced in spite of the noticeable discrepancy in peak width in the high frequency region. With doping, both the Li and H vibrations soften, as plotted in the figure 6.

The calculated EPC parameter λ for n-doped LiH with dc together with critical temperature T_c are given in table 2. It is predicted that λ will increase significantly with increasing dc, thus resulting in an increase of the superconducting transition temperature. In this study, a rigorous

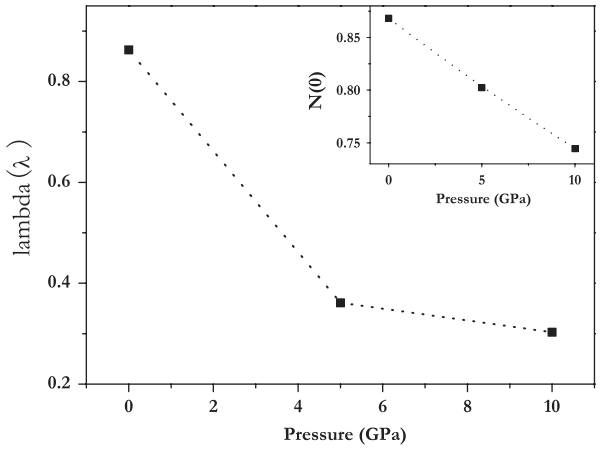

Figure 7. The pressure dependence of λ for n-doped LiH with $e_v = 2.06$. The inset represents the variation of $N(0)$ (unit: states Ryd^{-1} /spin· unit cell) with pressure. The dotted lines through the theoretical data points are a guide for the eye.

form

$$T_c = \frac{\omega_{\log}}{1.2} \exp\left[\frac{-1.04(1+\lambda)}{\lambda - \mu^*(1+0.62\lambda)}\right] \tag{4}$$

was used to estimate T_c. The increasing trend of λ with dc for n-doped LiH can be understood as follows. The EPC λ can be approximated by

$$\lambda \approx \frac{N(0)\langle I^2\rangle}{M\langle\omega^2\rangle} \tag{5}$$

where $\langle I^2\rangle$ is the average square of the electron–phonon matrix element, which is related to the phonon linewidth, M is the ionic mass, and $\langle\omega^2\rangle$ is a characteristic phonon frequency averaged over the phonon spectrum. The addition of a small amount of donor atoms to LiH has two significant effects. First, it affects the phonon spectrum essentially by decreasing the phonon frequency. Second, the n-doped LiH becomes more metallic with increasing dc as indicated by the increase in $N(0)$ (see table 2). Since the calculated phonon linewidth (not shown) does not change appreciably with dc, the increase of λ is attributed to the combined effect of phonon softening and the increased electron density of states at the Fermi level.

The effect of pressure on λ for n-doped LiH with $e_v = 2.06$ is depicted in figure 7. The λ of n-doped LiH is found to decrease with pressure. At ambient pressure, the T_c is estimated to be 7.78 K. At 5 GPa, the calculated λ of 0.361 corresponds to a T_c of 1.22 K and at 10 GPa the calculated λ of 0.303 results in a T_c of 0.36 K. Significantly, the present calculations indicate that T_c should have a strong dependence on pressure. As shown in the table 2, $N(0)$ decreases with increasing pressure. This behavior combined with an increase in phonon frequency at high pressure contributes to the decrease in T_c. This phenomenon is consistent with that for Nb, Bi, Pb, Sn, Al [30], MgB_2 [31], and boron-doped diamond [10] and in contrast to that for Li, Ca, Sr, V, La, Y, Lu, Sc, S, P [30], and MgC_xNi_3 [32].

The phonon linewidth that is one indicator of the mode-specific contribution to T_c along several high symmetry directions for n-doped LiH with $e_v = 2.06$ is present in figure 8. The calculated phonon linewidths of the acoustic modes are very small at all q-vectors, indicating a negligible contribution to the EPC from these modes. In contrast, the transverse optical (TO) and longitudinal optical (LO) phonon modes have large contributions to the EPC along the

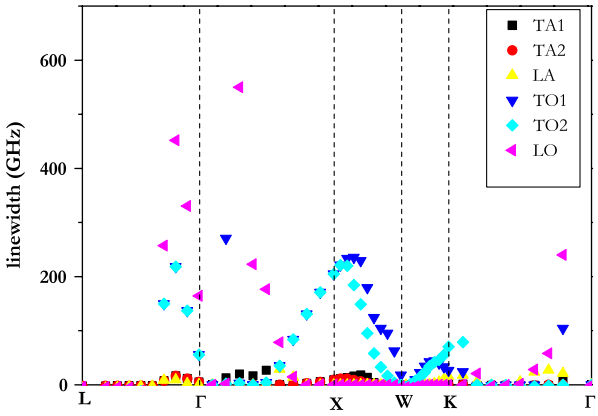

Figure 8. The phonon linewidth due to EPC for n-doped LiH at $e_v = 2.06$ along several high symmetry directions in the BZ.

Γ–X–W–K directions and at the zone center, respectively. This indicates that optical phonons dominate the EPC for the n-doped LiH.

As a dopant to LiH, beryllium seems to be a good candidate, because Be^{2+} has a similar size to Li^{+}. Since LiH is an ionic system, charge compensation implies that there will be hydrogen vacancies [33]. The view of metallic hydrogen in the form of metal hydrides has also been put forward by Overhauser [34]. He analyzed the structure of $LiBeH_3$ and $LiBeH_4$ and suggested that if these compounds are metallic then they could be high temperature superconductors. We argue, on the basis of the current prediction, that the doping of compounds (particularly H abundant compounds) with low Z elements is an efficient way to pursue high temperature superconductors. By all appearances, experimental efforts are needed to clarify the current prediction, and to further explore doped superconductors.

4. Conclusions

The electronic structure, lattice dynamics, and EPC for n-doped LiH have been studied using density functional theory within the VCA and supercell methods as regards electronic properties. For the current VCA calculation of n-doped LiH, essential properties of n-doped LiH such as the increase of the lattice parameter with increasing dc, and the pressure induced decrease of T_c are well simulated. It is found that the superconducting temperature T_c is 7.78 K with $e_v = 2.06$ at ambient pressure, indicating that n-doped LiH might show superconducting behavior. The increase of λ with dc for n-doped LiH is attributed to the phonon softening and the increased electron density of states at the Fermi level. From the phonon linewidth calculations, the optical phonon mode is found to dominate the EPC for n-doped LiH. To verify the currently predicted superconductivity of n-doped LiH, accurate experimental measurements on n-doped LiH are needed.

Acknowledgments

We thank for financial support the China 973 Program under grant No. 2005CB724400, the National Nature Science Associate Foundation of China under Grant No. 10676011, the National Doctoral Foundation of China Education Ministry under Grant No. 20050183062, the

Scientific Research Foundation for the Returned Overseas Chinese Scholars, State Education Ministry; the Program for 2005 New Century Excellent Talents in University, and the 2006 Project for Scientific and Technical Development of Jilin Province. Most of the calculations in this work were made using the Quantum-ESPRESSO package [35].

References

[1] Shpilrain E E, Yakimovich K A, Melnikova M E and Polishchuk A Y 1987 *Thermophysical Properties of Lithium Hydride, Deuteride, Tritide and of Their Solutions with Lithium* (New York: American Institute of Physics)
[2] Hama J, Suito K and Kawakami N 1989 *Phys. Rev.* B **39** 3351
[3] Ahuja R, Eriksson O and Johansson B 1999 *Physica* B **265** 87
[4] Loubeyre P, Toullec R L, Hanfland M, Ulivi L, Datchi F and Hausermann D 1998 *Phys. Rev.* B **57** 10403
[5] Islam A K 1993 *Phys. Status Solidi* b **180** 9
[6] McMillan W L 1968 *Phys. Rev.* **167** 331
[7] Zavt G S, Kalder K A, Kuusman I L, Lushichik Ch B, Plekhanov V G, Cholakh S O and E'varestov P A 1976 *Sov. Phys.—Solid State* **18** 1588
[8] Kondo Y and Asaumi K 1988 *J. Phys. Soc. Japan* **57** 367
[9] Nordheim L 1931 *Ann. Phys., Lpz.* **9** 607
[10] Ma Y M, Tse J S, Cui T, Klug D D, Zhang L J, Xie Y, Niu Y L and Zou G T 2005 *Phys. Rev.* B **72** 014306
[11] Baroni S, Giannozzi P and Testa A 1987 *Phys. Rev. Lett.* **58** 1861
[12] Giannozzi P, de Gironcoli S, Pavone P and Baroni S 1991 *Phys. Rev.* B **43** 7231
[13] Perdew J P, Burke K and Ernzerhof M 1996 *Phys. Rev. Lett.* **77** 3865
[14] Monkhorst H J and Pack J D 1976 *Phys. Rev.* B **13** 5188
[15] Savrasov S Y 1922 *Phys. Rev. Lett.* **69** 2819
[16] de Gironcoli S 1995 *Phys. Rev.* B **51** 6773
[17] Savrasov S Y, Savrasov D Y and Andersen O K 1994 *Phys. Rev. Lett.* **72** 372
[18] Methfessel M and Paxton A T 1989 *Phys. Rev.* B **40** 3616
[19] Allen P B 1972 *Phys. Rev.* B **6** 2577
[20] Allen P B and Silberglitt R 1974 *Phys. Rev.* B **9** 4733
[21] Schrieffer J R 1964 *Theory of Superconductivity* (New York: Benjamin)
[22] Murnaghan F D 1944 *Proc. Natl Acad. Sci. USA* **30** 244
[23] Perdew J P and Wang Y 1992 *Phys. Rev.* B **45** 13244
[24] Perdew J P and Zunger A 1981 *Phys. Rev.* B **23** 5048
[25] Roma G, Bertoni C M and Baroni S 1996 *Solid State Commun.* **98** 203
[26] Rodriguez C O and Kunc K 1989 *J. Phys.: Condens. Matter* **1** 1601
[27] Bellaiche L, Wei S-H and Zunger A 1997 *Appl. Phys. Lett.* **70** 3558
[28] Chen C, Wang E G, Cu Y M, Bylander D M and Kleinman L 1998 *Phys. Rev.* B **57** 3753
[29] Zemlianov M G, Brovman E G, Chernoplekov N A and Shitikov Yu L 1965 *Inelastic Scattering of Neutrons* vol II (Vienna: IAEA) p 431
[30] Buzea C and Robbie K 2005 *Supercond. Sci. Technol.* **18** R1 and reference therein
[31] Shao Y and Zhang X 2004 *J. Phys.: Condens. Matter* **16** 1103 and reference therein
[32] Yang H D, Mollah S, Huang W L, Ho P L, Liu C J, Lin J-Y and Zhang Y-L 2003 *Phys. Rev.* B **68** 092507
[33] Yu R and Lam P K 1988 *Phys. Rev.* B **37** 8730
[34] Overhauser A W 1987 *Phys. Rev.* B **35** 411
[35] Baroni S, Dal Corso A, de Gironcoli S, Giannozzi P, Cavazzoni C, Ballabio G, Scandolo S, Chiarotti G, Focher P, Pasquarello A, Laasonen K, Trave A, Car R, Marzari N and Kokalj A http://www.pwscf.org